

Isomeric Effects of Solution Processed Ladder-Type Non-Fullerene Electron Acceptors

Yongxi Li,^{a,c} Lian Zhong,^{b,e} Jiu-Dong Lin,^a Fu-Peng Wu,^a Hai-Jun Bin,^b Zhanjun Zhang,^e Lai Xu,^{a} Zuo-Quan Jiang,^a Zhi-Guo Zhang,^{b*} Feng Liu,^{d,f*} Thomas P. Russell,^f Yongfang Li,^{b,e} Liang-Sheng Liao,^{a*} Stephen R. Forrest,^{c*}*

^aJiangsu Key Laboratory for Carbon-Based Functional Materials & Devices, Institute of Functional Nano & Soft Materials (FUNSOM), Soochow University, Suzhou, Jiangsu 215123, China.

^bBeijing National Laboratory for Molecular Sciences, Institute of Chemistry, Chinese Academy of Sciences, Beijing 100190, China.

^cDepartment of Electrical Engineering and Computer Science, University of Michigan, Ann Arbor, Michigan 48109, USA.

^dDepartment of Physics and Astronomy, and Collaborative Innovation Center of IFSA (CICIFSA), Shanghai Jiaotong University, Shanghai 200240, P. R. China

^eUniversity of Chinese Academy of Sciences, Beijing 100049, China.

^fDepartment of Polymer Science and Engineering, University of Massachusetts, Amherst, MA 01003, USA.

Corresponding author: Dr Stephen R. Forrest, E-mail: stevefor@umich.edu

This is the author manuscript accepted for publication and has undergone full peer review but has not been through the copyediting, typesetting, pagination and proofreading process, which may lead to differences between this version and the Version of Record. Please cite this article as doi: 10.1002/solr.201700107

I. INTRODUCTION

The power conversion efficiencies (*PCE*) of organic photovoltaics (OPVs) have surpassed 12% in single junctions^[1], in part due to the development of non-fullerene acceptors (NFAs)^[2-16]. Considerable effort has focused on developing NFAs to overcome deficiencies of the commonly used fullerenes, such as their relatively low optical absorption in the visible and near infrared (NIR), a limited ability to modify their ionization and gap energies, and high-cost synthesis and purification processes. The ability, however, to predict device function from the NFA structure is relatively limited due to a lack of understanding of the structure-property relationships of these emerging materials.

Isomeric effects play a significant role in governing electronic structure, molecular stacking and device performance^[17-21] since they can determine the extent of conjugation along the molecular backbone. For example, naphthodithiophene (NDT) isomers used in organic field effect transistors have both linear- and angular-isomers with distinctly different electronic and crystal structures^[17]. Furthermore, recent studies have considered a series of isomorphous small molecule donors^[22-23]. While their molecular structures are similar, the symmetrical and asymmetrical configurations of the conjugated skeletons result in large differences in molecular ordering, dipole direction and OPV efficiency.

Here, we reveal the role that electronic structure plays in determining charge transfer and electron coupling due to orbital interactions by comparing the electronic

structures both in the solid state and at the molecular levels of two isomers. One of the materials is a thiophene-fused ladder acceptor ^[6, 24-32], represented by (4,4,9,9-tetrakis(4-hexylphenyl)-4,9-dihydro-s-indaceno[1,2-b:5,6-b']dithieno[3,2-b]thiophene-2,7-diyl) bis(2-(3-oxo-2,3-dihydroinden-1-ylidene)malononitrile) (IT-IC)^[33], which has attracted interest in view of its suitability for use in OPVs due to its visible light absorption and high charge carrier mobility^[1, 3, 34-41]. The core unit of IT-IC, indacenodithieno[3,2-b]thiophene (IDTT) is a highly planar conjugated structure. A similar ladder type molecule: dithienyl[1,2-b:4,5-b']benzodithiophene (BDCPDT **Scheme 1**) that is isoelectronic with IDTT has also been predicted to be a promising core for organic semiconductors^[18, 42, 43]. We compare the electronic and morphological properties of IT-IC with a planar BDCPDT-based acceptor-donor-acceptor (a-d-a) NFA (BDT-IC, **Scheme 1b**, the details of synthesis see Supplementary Information (**SI**)). The core structures of BDCPDT and IDTT are isomeric with four, linearly fused thiophenes, two cyclopentadienes and one benzene ring. We find differences in the distribution of electron density of the highest occupied molecular (HOMO) and lowest unoccupied molecular orbitals (LUMO) of IT-IC and BDT-IC. Antibonding interactions between atomic orbitals are found in IT-IC, which prevent substantial overlap between neighboring molecules, thereby resulting in disorder in the solid state. In contrast, BDT-IC exhibits a higher electron density and more compact crystal packing, leading to stronger inter- and intramolecular charge transfer with a reduced energy gap. Moreover, the improved order of BDT-IC acceptor combined with the large band gap polymer donor poly[2,6-(4,8-bis (5-(tripropylsilyl)thiophen-2-yl)benzo[1,2-b:4,5-b']dithiophene-alt-4,7-

Bis(5-thiophen-2-yl)-2-(2-hexyldecyl)-5,6-difluoro-2H-benzo[d]-[1,2,3]triazole(J71)

result in OPVs with power conversion efficiencies of $PCE = 10.5 \pm 0.4\%$, which to our knowledge are the highest values for as-cast solution-based devices.

We point out that recently, Chen and co-workers also reported a high efficiency solar cell based on BDT-IC after solvent vapor annealing^[43]. In our work, the significant impacts of isomeric effects on electronic structures and crystal properties of the IT-IC and BDT-IC isomers are revealed, and the structure-property relationships thus presented improve our understanding of ladder-type structures.

II. RESULTS

Chemical/Thermal Properties.

The chemical structural formulae of J71, IT-IC and BDT-IC are shown in **Figure 1a**. BDT-IC is soluble in dichloromethane (DCM), chloroform (CF), chlorobenzene (CB), and *ortho*-dichlorobenzene (*o*-DCB), all at room temperature. Moreover, BDT-IC shows relatively good solubility in halogen-free solvents such as tetrahydrofuran (THF), *o*-xylene and 1,2,4-trimethylbenzene, which is beneficial for roll-to-roll printing of large-area modules due to the need for substantial quantities of less toxic solvents. Thermal properties were investigated by thermal gravimetric analysis performed under nitrogen. BDT-IC has a decomposition temperature (5% weight loss) of 325 °C (**Figure S1** in SI).

Photo-Physical and Electrochemical Properties.

Thin film UV-Vis absorption spectra of J71, IT-IC and BDT-IC are shown in **Figure 1b**. BDT-IC has an absorption band spanning wavelengths between $\lambda = 550$ nm

and 750 nm in dilute DCM solution, with a maximum extinction coefficient of $1.4 \times 10^5 \text{ M}^{-1} \text{ cm}^{-1}$ at $\lambda = 693 \text{ nm}$ (**Figure S2** in SI). This is red-shifted and slight higher compare to IT-IC ($1.3 \times 10^5 \text{ M}^{-1} \text{ cm}^{-1}$ at 664 nm ^[33]). The red-shifted absorption is attributed to the increased internal charge transfer by the introduction of a stronger electron-donating moiety of the BDCPDT unit in this a-d-a type electron acceptor. Notably, the thin film absorption spectrum of BDT-IC is red-shifted by 40 nm, which may be due to the aggregation. The optical energy gap (E_g) of BDT-IC extracted from its long wavelength absorption edge in the solid-state is $1.53 \pm 0.02 \text{ eV}$ (**Table 1**), which is 0.06 eV smaller than for IT-IC ($1.59 \pm 0.02 \text{ eV}$). The absorption edge of J71 is located at 640 nm.

The energetics of J71, BDT-IC and IT-IC were investigated using cyclic voltammetry to obtain HOMO and LUMO energies (E_{HOMO} and E_{LUMO} , respectively) listed in **Table 1**, with voltammetry data in **Figure S3** in Supplementary Information (SI). As shown in **Figure 1c**, BDT-IC exhibits a higher HOMO energy but almost the same LUMO energy compared with IT-IC, implying that changes in the a-d-a molecular backbone affects E_{HOMO} but not E_{LUMO} . This allows for an increased cutoff wavelength without reducing the open circuit voltage (V_{oc}) in OPVs.

Molecular orientation and crystallinity.

Grazing incidence x-ray diffraction (GIXD) was used to investigate the influence of isomerization on the thin film morphology (see in **Figure 2**). It is clear that the IT-IC thin film is disordered, with only weak diffraction peaks at 0.34 \AA^{-1} and 1.77 \AA^{-1} (summarized in **Table 2**). IT-IC diffraction shows the (100) peak in the in-plane (IP) direction at 0.34 \AA^{-1} (corresponding to an inter-planar spacing of $d_{100} = 18.5 \pm 0.4 \text{ \AA}$) and

the (010) plane is in the out-of-substrate-plane (OOP) direction at 1.77 \AA^{-1} ($d_{010} = 3.5 \pm 0.1 \text{ \AA}$). Due to considerable disorder of IT-IC spin-cast films, we were unable to accurately estimate the crystal coherence length. On the other hand, The BDT-IC showed a narrow diffraction peak at 1.81 \AA^{-1} in the perpendicular direction, corresponding to ordered π -stacking at $3.4 \pm 0.1 \text{ \AA}$, and an unambiguous clear crystal coherence length of $\zeta = 4.5 \pm 0.2 \text{ nm}$. Furthermore, the (100) peak at 0.32 \AA^{-1} was observed in the IP direction, corresponding to a lamellar distance of $19.6 \pm 0.5 \text{ \AA}$ and $\zeta = 22.0 \pm 0.6 \text{ nm}$. Therefore, we conclude that configurational isomerization rotates the molecule from upstanding to flat-lying on the substrate with increased crystallite size.

Organic field effect transistor (OFET) device performance.

Top-gate/bottom-source and drain-contact thin film field effect transistors (TFTs) with BDT-IC and IT-IC channels were used to evaluate the charge transport behavior. Both acceptors exhibited n -type transport (**Figure S4** in SI) with well-defined linear and saturation regimes. The transfer characteristics show high off-current at large V_d due to the ambipolar charge transport properties of these two acceptors. The mobilities in the saturation regimes were 0.46 ± 0.03 and $0.11 \pm 0.01 \text{ cm}^2 \text{ V}^{-1} \text{ s}^{-1}$ for BDT-IC and IT-IC, respectively. The electron mobilities are attributed to the different electronic structures and crystal packing habits in the thin films.

Organic solar cell device performance.

The performance of OPVs based on IT-IC and BDT-IC combined with a polymer donor (named J71) are summarized in **Table 3**. The devices were fabricated from chloroform solution with the following structure: ITO/PEDOT:PSS (40 nm) /J71:BDT-IC

or IT-IC (100 nm) /PDINO (10 nm) /Al (100 nm). Here, PDINO (perylene diimide functionalized with amino *N*-oxide) is the cathode buffer exciton blocking layer^[44]. The details of fabrication are found in Methods (SI). The optimized devices for J71:BDT-IC were spin-coated from chloroform solution with a 1:1.2 donor:acceptor (D:A) weight ratio. The optimized device had $PCE = 10.5 \pm 0.4\%$ with $V_{oc} = 0.92 \pm 0.01$ V, short circuit current $J_{sc} = 17.3 \pm 0.4$ mA cm⁻², and fill factor $FF = 0.66 \pm 0.03$ at 1 sun intensity, simulated AM1.5G illumination (see **Table 3**). The efficiency histogram in **Figure 3** shows >70% of the devices (among 30 devices) have PCE higher than 9.8%. In contrast, the as-cast devices based on IT-IC exhibited best $PCE = 9.0 \pm 0.3\%$ with $V_{oc} = 0.96 \pm 0.01$ V and decreased $J_{sc} = 14.8 \pm 0.5$ mA cm⁻² and $FF = 0.64 \pm 0.03$.

The EQE vs. wavelength for the ladder-type molecules are provided in **Figure 3b**. The long wavelength cut off of the BDT-IC based OPV is at $\lambda = 810$ nm, which is red-shifted by ~40 nm compared to the IT-IC based device. The EQE of the BDT-IC based device reaches 70%, between 450 nm and 780 nm. The J_{sc} inferred from the integrated EQE is 16.5 mA cm⁻², which is within 4% of that measured from the simulated 1 sun, AM1.5G solar illuminated photovoltaic J - V measurement.

III. DISCUSSION

The different positions of cyclopentadiene result in different crystalline morphologies that lead to differences in the charge mobility. We also speculate that the distributions of the electron densities of the HOMO and LUMO play an important role in differentiating their charge carrier transport properties. Density functional theory (DFT)

calculations at the GGA:PW91/TZP level were performed to investigate the geometric and electronic properties of IT-IC and BDT-IC^[45]. Interestingly, as shown in **Figure 4**, the distribution of electron densities of the HOMOs and LUMOs for IT-IC and BDT-IC are different. Previous studies have found that the larger atomic radius of sulfur (S) compared to carbon (C) results in increased intermolecular interactions in ladder-type molecules^[17, 46]. As a result of antibonding interactions between atomic orbitals, the electron densities on the S atoms in IT-IC are also small. On the other hand, the large electron densities on the S atoms in both the HOMO and LUMO levels of the BDT-IC provide substantial overlap between neighboring molecules in the solid state, giving rise to increased crystallinity, and thus improved charge carrier transport. This agrees with the observation that the reduced π -stacking distance of BDT-IC results in a five times higher electron mobility than IT-IC. We expect that the differences in the electronic structures of these two molecules originate from their fused-ring frameworks. Compared to the thieno[3,2-b]thiophene in IT-IC, it is easier for the S in the cyclopentadithiophene unit in BDT-IC to supply two π -electrons, resulting in a comparatively high electron density. Also, BDT-IC has a planar structure with torsion angles $< 2^\circ$ that facilitate π -electron delocalization.

The blends of J71:IT-IC and J71:BDT-IC were also characterized by GIXD, as shown in **Figure 5**. J71 in the pure film showed a prominent (100) diffraction peak at 0.29 \AA^{-1} in the IP direction. The lamellar distance is $21.6 \pm 0.5 \text{ \AA}$ and $\zeta = 7.0 \pm 0.2 \text{ nm}$ (**Table 3**). An intense π -stacking diffraction peak is seen in the OOP direction located at 1.67 \AA^{-1} , giving a π -stacking distance of $3.8 \pm 0.1 \text{ \AA}$ nm with $\zeta = 2.9 \pm 0.1 \text{ nm}$. In J71:BDT-

IC blend thin films, the (100) diffraction peak is dominated by contributions from BDT-IC since the (100) diffraction peak is located at 0.32 \AA^{-1} . In this case, the presence of BDT-IC guides the blend morphology. Furthermore, The BT-CIC shows improved π -stacking, as seen from the (010) diffraction peak at 1.76 \AA^{-1} in the perpendicular direction, which indicates a reduced π -stacking distance compared to the J71:IT-IC film (1.62 \AA^{-1})^[36]. Recently, studies by Ade and co-workers predicted that face-on orientation in the blend film is a general feature of high-performance bulk heterojunction organic solar cells due to the reduction of recombination of excitons during charge separation^[47]. The combination of the preferred face-on orientation and the tight π -stacking of the BDT-IC blends, can improve exciton dissociation and/or charge transport, thus enhancing performance.

From **Table 3**, the improvement of J_{sc} in the BDT-IC vs. the IT-IC device is attributed to the red-shifted absorption that provides solar spectral response into the near-infrared (NIR). The length scale of phase separation of J71:BDT-IC was studied using resonant soft x-ray diffraction. A well-defined phase separation at 0.007 \AA^{-1} corresponding to a distance of 90 nm is observed (see **Figure 5c**). Such a large length scale in non-fullerene-based solar cells gives rise to a high J_{sc} . This result is also consistent with transmission electron microscopy and atomic force microscopy (AFM) images of the blends (see **Figure S5**). Fiber-like features are observed in the topographic image of the J71:BDT-IC blend with larger root-mean-square (RMS) roughness of 1.13 than J71:IT-IC blend (0.53). The roughness of the blend results in increased contact area between the active layer and the interfacial layer, which may result in efficient exciton

dissociation at the interface. We also observe an increased FF in the J71:BDT-IC based device. The hole and electron mobilities of the blend were estimated using the space charge limited current (SCLC) method (see SI) to be $1.13\pm 0.06\times 10^{-4}$ $\text{cm}^2 \text{V}^{-1} \text{s}^{-1}$ and $1.90\pm 0.09\times 10^{-4}$ $\text{cm}^2 \text{V}^{-1} \text{s}^{-1}$, respectively for J71:BDT-IC, corresponding to nearly balanced charge transport ($\mu_e/\mu_h = 1.7$).

Many high-performance solution-processed solar cells require often-complicated post-cast treatments or additives that can lead to irreproducibility and added cost [39]. However, the BDT-IC-based solar cells can achieve high performance without these treatments. Typically, for fullerene-based OPVs, additives or post-cast treatments are used to increase polymer crystallinity while reducing fullerene domain size^[48]. Since ladder-type NFAs have a high solubility in organic reagents compared with fullerenes, the blends can be uniform. However, there may be a residual phase separation when mixed with the donors, which reduces the charge separation efficiency. One approach to mitigate this issue is increasing the NFA crystallinity. This is why BDT-IC provides improved OPV performance compared with IT-IC without post-cast treatments or additives.

IV. CONCLUSIONS

Two isomeric non-fullerene acceptors featuring a large fused ring ladder-type structural motif were designed and synthesized for OPVs. The isomer BDT-IC shows a smaller energy gap, stronger intermolecular interactions and more crystallinity than IT-IC. Specifically, BDT-IC exhibited five times higher electron mobility, which leads to a reduced charge recombination. Moreover, as-cast OPVs without additional treatments or

additives employing BDT-IC paired with the J71 donor exhibited $PCE = 10.5 \pm 0.4\%$. The significant impacts of isomeric effects on electronic structure and crystal properties of the IT-IC and BDT-IC isomers are revealed. These studies help to elucidate the structure-property relationships of high performance NFAs, providing insights for the future rational design of improved non-fullerene acceptor materials.

V. ACKNOWLEDGMENTS

This work is funded by the Collaborative Innovation Center of Suzhou Nano Science and Technology (Nano-CIC) and by the Priority Academic Program Development of Jiangsu Higher Education Institutions (PAPD). YL and SRF were funded in part by the Office of Energy Efficiency and Renewable Energy (EERE), U.S. Department of Energy, under Award Number DE-EE0006708 and by the Department of the Navy, Office of Naval Research under Award No. N00014-17-1-2211. TPR was supported by the U.S. Office of Naval Research under contract N00014-15-1-2244. GIXD measurements were carried out at beamline 7.3.3 and 11.0.1.2 at the Advanced Light Source, and Molecular Foundry, Lawrence Berkeley National Laboratory, which was supported by the U.S. Department of Energy, Offices of Science, and Basic Energy Sciences. This work was also supported by the National Natural Science Foundation of China (21504062 and 21603155). We thank Prof. Jie-Yu Wang and Hio-Ieng, Un for transistor measurements. Yongxi Li and Lian Zhong contributed equally to this work.

REFERENCES

- [1] S. Li, L. Ye, W. Zhao, S. Zhang, S. Mukherjee, H. Ade, J. Hou, *Adv. Mater.* **2016**, 28, 9423.
- [2] W. Zhao, D. Qian, S. Zhang, S. Li, O. Inganäs, F. Gao, J. Hou, *Adv. Mater.* **2016**, 28, 4734.
- [3] Y. Yang, Z.-G. Zhang, H. Bin, S. Chen, L. Gao, L. Xue, C. Yang, Y. Li, *J. Am. Chem. Soc.* **2016**, 138, 15011.
- [4] D. Meng, H. Fu, C. Xiao, X. Meng, T. Winands, W. Ma, W. Wei, B. Fan, L. Huo, N. L. Doltsinis, Y. Li, Y. Sun, Z. Wang, *J. Am. Chem. Soc.* **2016**, 138, 10184.
- [5] Y. Li, L. Zhong, B. Gautam, H.-J. Bin, J.-D. Lin, F.-P. Wu, Z. Zhang, Z.-Q. Jiang, Z.-G. Zhang, K. Gundogdu, Y. Li, L.-S. Liao, *Energy Environ. Sci.* **2017**, 10, 1610.
- [6] Y. Li, L. Zhong, F.-P. Wu, Y. Yuan, H.-J. Bin, Z.-Q. Jiang, Z. Zhang, Z.-G. Zhang, Y. Li, L.-S. Liao, *Energy Environ. Sci.* **2016**, 9, 3429.
- [7] S. X. Li, W. Q. Liu, M. M. Shi, J. Q. Mai, T. K. Lau, J. H. Wan, X. H. Lu, C. Z. Li, H. Z. Chen, *Energy Environ. Sci.* **2016**, 9, 604.
- [8] D. Baran, T. Kirchartz, S. Wheeler, S. Dimitrov, M. Abdelsamie, J. Gorman, R. S. Ashraf, S. Holliday, A. Wadsworth, N. Gasparini, P. Kaienburg, H. Yan, A. Amassian, C. J. Brabec, J. R. Durrant, I. McCulloch, *Energy Environ. Sci.* **2016**, 9, 3783.
- [9] Y. Zhong, M. T. Trinh, R. Chen, G. E. Purdum, P. P. Khlyabich, M. Sezen, S. Oh, H. Zhu, B. Fowler, B. Zhang, W. Wang, C. Y. Nam, M. Y. Sfeir, C. T. Black, M. L. Steigerwald, Y. L. Loo, F. Ng, X. Y. Zhu, C. Nuckolls, *Nat. Commun.* **2015**, 6, 8242.
- [10] C. B. Nielsen, S. Holliday, H.-Y. Chen, S. J. Cryer, I. McCulloch, *Acc. Chem. Res.* **2015**, 48, 2803.

- [11] Y. Lin, X. Zhan, *Mater. Horiz.* **2014**, *1*, 470.
- [12] G. Zhang, G. Yang, H. Yan, J.-H. Kim, H. Ade, W. Wu, X. Xu, Y. Duan, Q. Peng, *Adv. Mater.* **2017**, DOI: 10.1002/adma.201606054.
- [13] J. Zhao, Y. Li, G. Yang, K. Jiang, H. Lin, H. Ade, W. Ma, H. Yan, *Nature Energy* **2016**, *1*, 15027.
- [14] O. K. Kwon, M. A. Uddin, J.-H. Park, S. K. Park, T. L. Nguyen, H. Y. Woo, S. Y. Park, *Adv. Mater.* **2016**, *28*, 910.
- [15] W. Chen, Q. Zhang, *J. Mater. Chem. C* **2017**, *5*, 1275.
- [16] Y. Zang, C.-Z. Li, C.-C. Chueh, S. T. Williams, W. Jiang, Z.-H. Wang, J.-S. Yu, A. K. Y. Jen, *Adv. Mater.* **2014**, *26*, 5708.
- [17] S. Shinamura, I. Osaka, E. Miyazaki, A. Nakao, M. Yamagishi, J. Takeya, K. Takimiya, *J. Am. Chem. Soc.* **2011**, *133*, 5024.
- [18] Y.-L. Chen, J.-Y. Hsu, F.-Y. Lin, Y.-Y. Lai, H.-C. Chou, Y.-J. Cheng, *J. Org. Chem.* **2016**, *81*, 2534.
- [19] I. Osaka, T. Abe, S. Shinamura, K. Takimiya, *J. Am. Chem. Soc.* **2011**, *133*, 6852.
- [20] S. W. Cheng, D. Y. Chiou, C. E. Tsai, W. W. Liang, Y. Y. Lai, J. Y. Hsu, C. S. Hsu, I. Osaka, K. Takimiya, Y. J. Cheng, *Adv. Funct. Mater.* **2015**, *25*, 6131.
- [21] J. Lee, H.-F. Chen, T. Batagoda, C. Coburn, P. I. Djurovich, M. E. Thompson, S. R. Forrest, *Nature Mater.* **2016**, *15*, 92.
- [22] C. J. Takacs, Y. Sun, G. C. Welch, L. A. Perez, X. Liu, W. Wen, G. C. Bazan, A. J. Heeger, *J. Am. Chem. Soc.* **2012**, *134*, 16597.

- [23] X. Che, C.-L. Chung, X. Liu, S.-H. Chou, Y.-H. Liu, K.-T. Wong, S. R. Forrest, *Adv. Mater.* **2016**, 28, 8248.
- [24] Y. Li, X. Liu, F.-P. Wu, Y. Zhou, Z.-Q. Jiang, B. Song, Y. Xia, Z.-G. Zhang, F. Gao, O. Inganäs, Y. Li, L.-S. Liao, *J. Mater. Chem. A* **2016**, 4, 5890.
- [25] Y. Li, D. Qian, L. Zhong, J. D. Lin, Z. Q. Jiang, Z. G. Zhang, Z. Zhang, Y. Li, L. S. Liao, F. Zhang, *Nano Energy* **2016**, 27, 430.
- [26] Y. Lin, Q. He, F. Zhao, L. Huo, J. Mai, X. Lu, C.-J. Su, T. Li, J. Wang, J. Zhu, *J. Am. Chem. Soc.* **2016**, 138, 2973.
- [27] H. Yao, Y. Cui, R. Yu, B. Gao, H. Zhang, J. Hou, *Angew. Chem. Int. Ed.* **2017**, 56, 3045.
- [28] S. Dai, F. Zhao, Q. Zhang, T.-K. Lau, T. Li, K. Liu, Q. Ling, C. Wang, X. Lu, W. You, *J. Am. Chem. Soc.* **2017**, 139, 1336.
- [29] F. Liu, Z. Zhou, C. Zhang, T. Vergote, H. Fan, F. Liu, X. Zhu, *J. Am. Chem. Soc.* **2016**, 138, 15523.
- [30] F. Liu, Z. Zhou, C. Zhang, J. Zhang, Q. Hu, T. Vergote, T. P. Russell, X. Zhu, *Adv. Mater.* **2017**, DOI: 10.1002/adma.201606574.
- [31] N. Qiu, H. Zhang, X. Wan, C. Li, X. Ke, H. Feng, B. Kan, H. Zhang, Q. Zhang, Y. Lu, *Adv. Mater.* **2017**, 29, 4964.
- [32] H. Yao, Y. Chen, Y. Qin, R. Yu, Y. Cui, B. Yang, S. Li, K. Zhang, J. Hou, *Adv. Mater.* **2016**, 28, 8283.
- [33] Y. Lin, J. Wang, Z.-G. Zhang, H. Bai, Y. Li, D. Zhu, X. Zhan, *Adv. Mater.* **2015**, 27, 1170.

- [34] L. Gao, Z. G. Zhang, H. Bin, L. Xue, Y. Yang, C. Wang, F. Liu, T. P. Russell, Y. Li, *Adv Mater* **2016**, 28, 8288.
- [35] H. Bin, Z.-G. Zhang, L. Gao, S. Chen, L. Zhong, L. Xue, C. Yang, Y. Li, *J. Am. Chem. Soc.* **2016**, 138, 4657.
- [36] H. Bin, L. Gao, Z.-G. Zhang, Y. Yang, Y. Zhang, C. Zhang, S. Chen, L. Xue, C. Yang, M. Xiao, Y. Li, *Nat. Commun.* **2016**, 7, 13651.
- [37] F. Yang, C. Li, W. Lai, A. Zhang, H. Huang, W. Li, *Mater. Chem. Front.* **2017**, DOI: 10.1039/C7QM00025A.
- [38] Y. Lin, F. Zhao, Q. He, L. Huo, Y. Wu, T. C. Parker, W. Ma, Y. Sun, C. Wang, D. Zhu, A. J. Heeger, S. R. Marder, X. Zhan, *J. Am. Chem. Soc.* **2016**, 138, 4955.
- [39] Y. Lin, Q. He, F. Zhao, L. Huo, J. Mai, X. Lu, C.-J. Su, T. Li, J. Wang, J. Zhu, Y. Sun, C. Wang, X. Zhan, *J. Am. Chem. Soc.* **2016**, 138, 2973.
- [40] H. Yao, L. Ye, J. Hou, B. Jang, G. Han, Y. Cui, G. M. Su, C. Wang, B. Gao, R. Yu, H. Zhang, Y. Yi, H. Y. Woo, H. Ade, J. Hou, *Adv. Mater.* **2017**, DOI: 10.1002/adma.201700254.
- [41] Y.-X. Xu, C.-C. Chueh, H.-L. Yip, F.-Z. Ding, Y.-X. Li, C.-Z. Li, X. Li, W.-C. Chen, A. K. Y. Jen, *Adv. Mater.* **2012**, 24, 6356.
- [42] Y.-L. Chen, C.-Y. Chang, Y.-J. Cheng, C.-S. Hsu, *Chem. Mater.* **2012**, 24, 3964.
- [43] B. Kan, H. Feng, X. Wan, F. Liu, X. Ke, Y. Wang, Y. Wang, H. Zhang, C. Li, J. Hou, Y. Chen, *J. Am. Chem. Soc.* **2017**, 139, 4929.
- [44] Z.-G. Zhang, B. Qi, Z. Jin, D. Chi, Z. Qi, Y. Li, J. Wang, *Energy Environ. Sci.* **2014**, 7, 1966.

- [45] G. t. Te Velde, F. M. Bickelhaupt, E. J. Baerends, C. Fonseca Guerra, S. J. van Gisbergen, J. G. Snijders, T. Ziegler, *J. Comput. Chem.* **2001**, *22*, 931.
- [46] K. Takimiya, S. Shinamura, I. Osaka, E. Miyazaki, *Adv. Mater.* **2011**, *23*, 4347.
- [47] J. R. Tumbleston, B. A. Collins, L. Yang, A. C. Stuart, E. Gann, W. Ma, W. You, H. Ade, *Nature Photon.* **2014**, *8*, 385.
- [48] Z. Li, K. Jiang, G. Yang, J. Y. Lai, T. Ma, J. Zhao, W. Ma, H. Yan, *Nat. Commun.* **2016**, *7*, 13094.

Author Manuscript

TABLES

Table 1. Optical and electrochemical properties of non-fullerene acceptors.

Material	λ_{\max}^a (nm)	E_g^b (eV)	HOMO ^c (eV)	LUMO ^c (eV)	μ_e^d (cm ² V ⁻¹ s ⁻¹)	λ^e (meV)
IT-IC	709	1.59	-5.58	-3.88	0.1	94
BDT-IC	739	1.53	-5.51	-3.90	0.5	93

^a Thin film measurement; ^bOptical energy gap; ^cFrom cyclic voltammetry measurement; ^dFrom OFET measurement; ^eReorganization energy.

Table 2. Grazing incidence x-ray diffraction results of J71, IT-IC and BDT-IC in neat and blend films.

Active Layer	$q_{(100)}$ (\AA^{-1})	$d_{(100)}$ (\AA)	$q_{(010)}$ (\AA^{-1})	$d_{(010)}$ (\AA)	$\zeta_{(100)}$ (nm)	$\zeta_{(010)}$ (nm)
IT-IC	0.34	18.5±0.4	1.77	3.5±0.1	-	-
BDT-IC	0.32	19.6±0.5	1.81	3.4±0.1	22.0±0.6	4.5±0.2
J71	0.29	21.6±0.5	1.67	3.8±0.1	7.0±0.2	2.9±0.1
J71:IT-IC ^a	-	-	1.62	3.88	-	-
J71:BDT-IC	0.32	19.6±0.5	1.76	3.5±0.1	-	-

^a Results from ref 36.

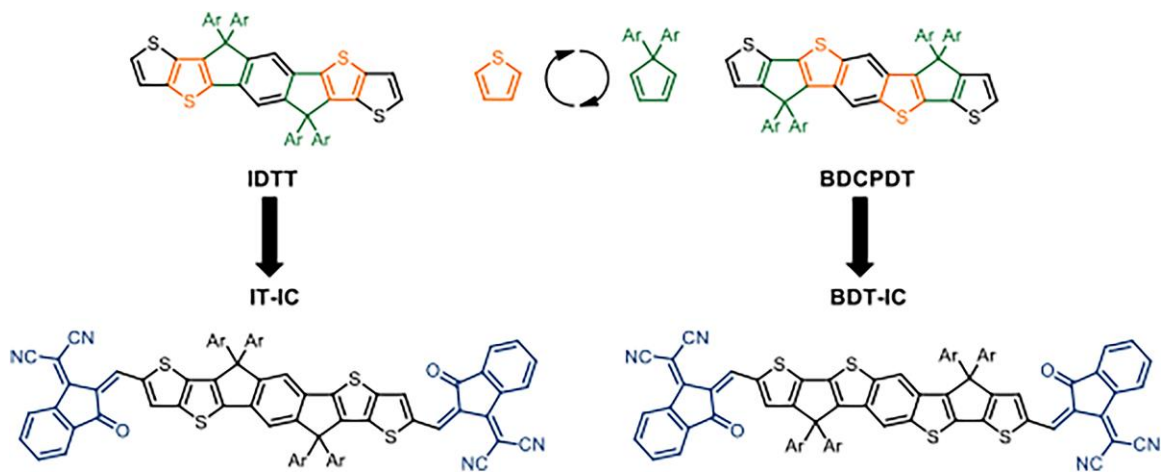
Table 3. Photovoltaic parameters of the as cast PSCs based on J71 as a donor and IT-IC/BDT-IC as an acceptor under the illumination of AM 1.5G, 100 mW cm⁻².

Active layer ^a	V_{oc} (V)	J_{sc} (mA cm ⁻²)	FF (%)	PCE ^b (%)
J71:IT-IC	0.96±0.01	14.8±0.5	63.6±3.4	9.0±0.3
J71:BDT-IC	0.92±0.01	17.3±0.4	65.5±2.9	10.5±0.4

^aAs deposited value; ^bValues are average PCEs from 30 devices

Author Manuscript

SCHEME AND FIGURE CAPTIONS



Scheme 1. Molecular design of the BDCPDT-based non-fullerene acceptor, BDT-IC. BDCPDT is isoelectronic with IDTT by re-organizing the alignment of thiophene and cyclopentadiene units.

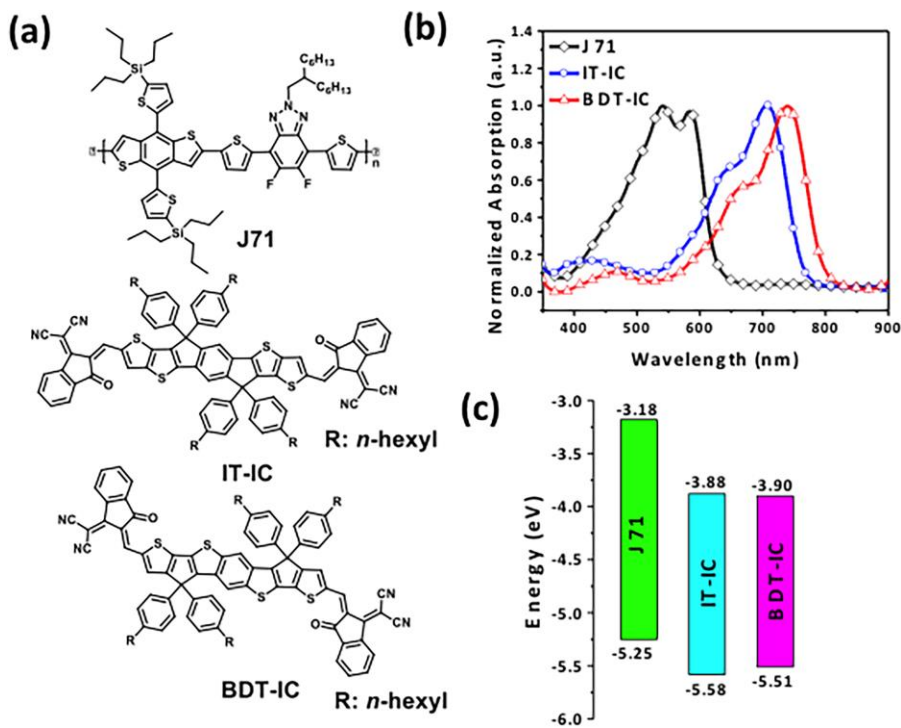


Figure 1. (a) Molecular structural formulae of J71, IT-IC and BDT-IC; (b) Normalized UV-Vis absorption spectra of J71, IT-IC and BDT-IC thin films; (c) Energy diagram of J71, IT-IC and BDT-IC relative to vacuum obtained from cyclic voltammetry measurements.

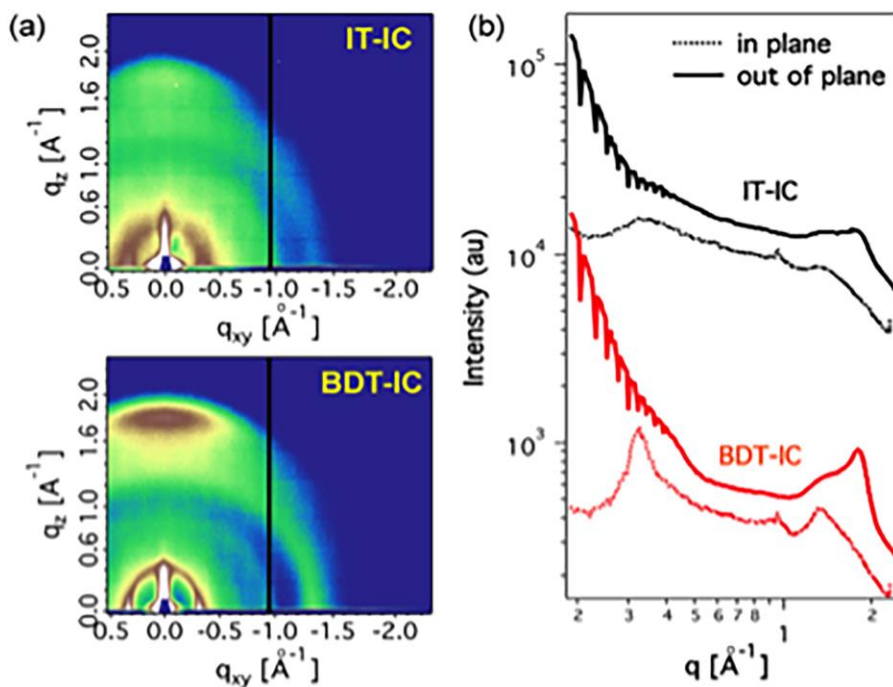


Figure 2. (a) Grazing incidence x-ray diffraction (GIXD) patterns of as-cast IT-IC and BDT-IC films; (b) In-plane (dotted line) and out-of-plane (solid line) x-ray scattering patterns extracted from the 2D GIXD images. Here, q is the scattering vector, q_{xy} is the in-plane direction and q_z is the out-of-plane direction.

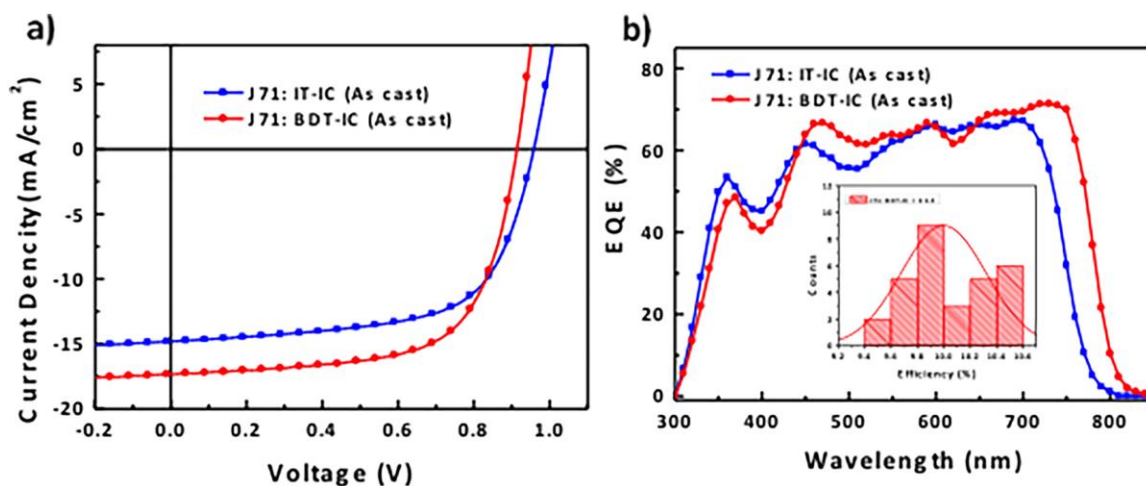


Figure 3. (a) Current-density-voltage characteristics, and (b) External quantum efficiency (*EQE*) spectra of the organic photovoltaic cells based on J71: IT-IC (1:1, w/w) and J71: BDT-IC (1:1.2, w/w). *Inset:* Histogram of efficiencies of organic photovoltaic cells (among 30 devices) based on J71: BDT-IC (1:1.2, w/w).

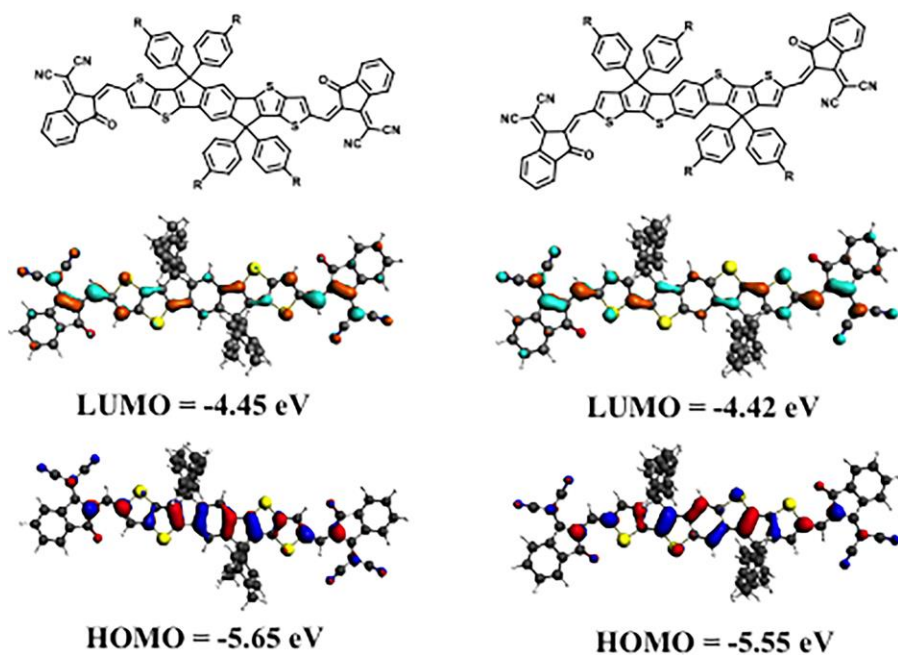


Figure 4. Calculated highest occupied molecular orbitals (HOMOs) and lowest unoccupied molecular orbitals (LUMOs) of IT-IC (left) and BDT-IC (right) from density functional theory using the TZP basis set at the with the GGA:PW91 level. Blue and red regions show the HOMOs along the of IT-IC and BDT-IC, the green and orange regions show the LUMOs along the of IT-IC and BDT-IC)

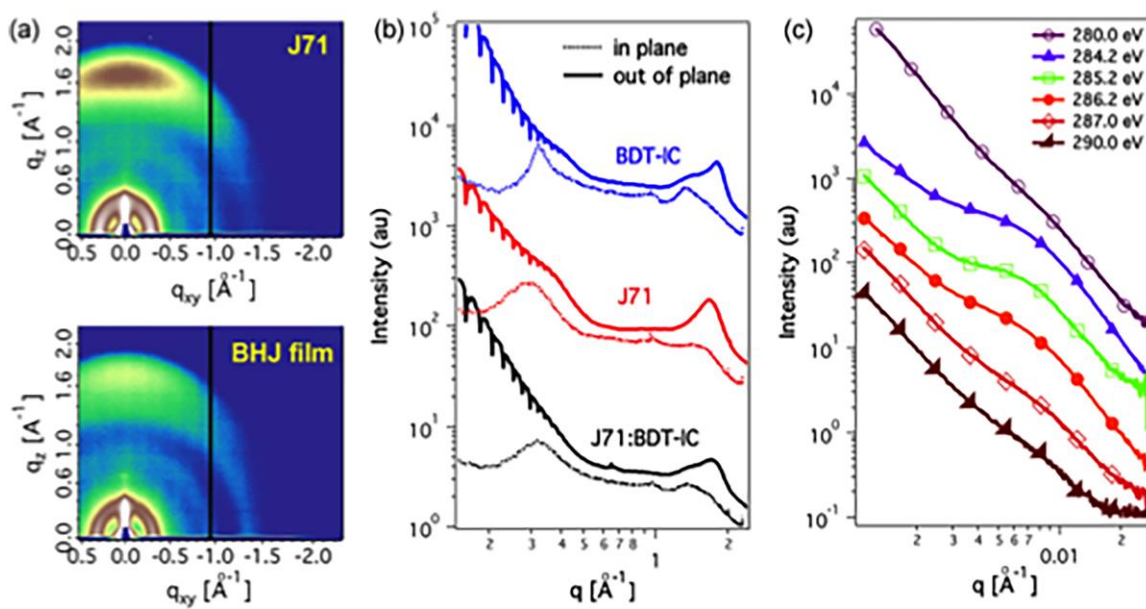


Figure 5. (a) Grazing incidence x-ray diffraction patterns; (b) patterns taken along the lines in (a), and (c) resonant soft x-ray scattering of J71, BDT-IC and J71:BDT-IC blends. Here, q is the scattering vector, q_{xy} is the in plane direction and q_z is the out of plane direction.